GKSS
FORSCHUNGSZENTRUM
in der HELMHOLTZ-GEMEINSCHAFT

Final Draft
of the original manuscript:

Gomes, D.; Marschall, R.; Pereira Nunes, S.; Wark, M.:
Development of polyoxadiazole nanocomposites for high temperature polymer electrolyte membrane fuel cells
In: Journal of Membrane Science (2008) Elsevier

DOI: 10.1016/j.memsci.2008.06.010

Development of Polyoxadiazole Nanocomposites for High Temperature Polymer Electrolyte Membrane Fuel Cells

Dominique Gomes[*,†], *Roland Marschall*[‡], *Suzana P. Nunes*[†], *Michael Wark*[‡]

[†]GKSS Research Centre Geesthacht GmbH, Institute of Polymer Research, Max Planck Str. 1, D-21502, Geesthacht, Germany, and [‡] Gottfried Wilhelm Leibniz Universität Hannover, Callinstrasse 3a, 30167, Hannover, Germany.

RECEIVED DATE (to be automatically inserted after your manuscript is accepted if required according to the journal that you are submitting your paper to)

TITLE RUNNING HEAD: Polyoxadiazole nanocomposites for PEMFCs

ABSTRACT: Novel nanocomposite membranes were prepared with sulfonated polyoxadiazole and different amounts of sulfonated dense and mesoporous (MCM-41) silica particles. It has been shown that particle size and functionality of sulfonated silica particles play an important role when they are used as fillers for the development of polymer

[*] Corresponding author. Email: dominique.gomes@gkss.de. Tel.: +49 04152 87 2472. Fax: +49 04152 87 2466.

[†] GKSS Research Centre Geesthacht GmbH

[‡] Gottfried Wilhelm Leibniz Universität Hannover

electrolyte nanocomposite membrane for fuel cells. No significant particle agglomerates were observed in all nanocomposite membranes prepared with sulfonated dense silica particles, as analyzed by SEM, AFM, TGA, DMTA and tensile tests. The T_g values of the composite membranes increased with addition of sulfonated silica, indicating an interaction between the sulfonic acid groups of the silica and the polyoxadiazole. Constrained polymer chains in the vicinity of the inorganic particles were confirmed by the reduction of the relative peak height of tan δ. A proton conductivity of 0.034 S cm^{-1} at 120°C and 25% RH, which is around two-fold higher than the value of the pristine polymer membrane was obtained.

TOC Summary and Graphic Template for Chemistry of Materials

Dominique Gomes*, Roland Marschall, Suzana P. Nunes, Michael Wark

Chem. Mater.

Development of Polyoxadiazole Nanocomposites for High Temperature Polymer Electrolyte Membrane Fuel Cells

Novel nanocomposite membranes prepared with sulfonated polyoxadiazole and homogeneously distributed sulfonated silica with particle nanosizes of 10-15 nm. (Left) Tapping mode AFM topography. (Right) Phase mode AFM image of the same area. In the phase contrast mode, the inorganic particles can be differentiated and assigned to the bright areas.

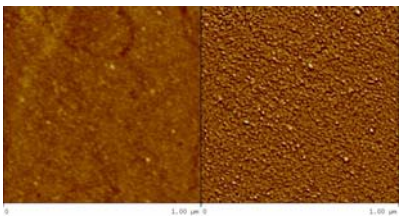

1. Introduction

Incorporation of inorganic particles or fillers into polymeric materials has been the subject of growing interest in different technological areas such as fuel cells,[1-15] gas separation process,[16-20] and others requiring materials with improved electrical, optical, or mechanical properties.[21-30] Interesting candidates with potentially unique properties are silica, aluminium oxide, zinc oxide, carbon nanotube, fullerene, zeolite and graphene. The range of applications of silica particles is continuously growing due to their high specific area, large porous volume, large mechanical and thermal stability and easy surface modification. Although nanoparticles exhibit a high potential of application in different research fields, there are still many limitations and challenges to be met such as the manufacturing route and surface

properties of nanoparticles, which influence the resulting degree of dispersion and interfacial adhesion with the polymer matrix. The main disadvantages of the incorporation of fillers to polymers are agglomeration of particles and formation of non-selective voids at the interface of the particles and the polymer matrix. However, the interfacial bonding between the nanofiller and the polymeric matrix can be improved by functionalizing the filler surface. Gomes et al.[4] have also obtained better dispersion and a rather good adhesion between inorganic domains and the polymer matrix after functionalizing inorganic silica particles with sulfonated hydroxytelechelic containing 1,3,4-oxadiazole units.

Oxadiazole-based polymers, like most thermally stable polymers, are good candidates for applications that require flame-resistance, fire-resistance or self-extinguishing properties. They present a combination of properties (such as mechanical strength, thermal and chemical stability) that makes them good candidates for application as high temperature fibers,[31] reinforcement materials,[32] graphitized fibers,[32] membrane materials for gas separation, ultrafiltration, reverse osmosis and fuel cell.[4,33] The Helmholtz-University group at GKSS has been developing polyoxadiazole-based nanocomposites for different applications.[34] Gomes et al. have recently shown their use as coating to prevent corrosion of metal surfaces.[35] In the fuel cell field, the development of highly effective membranes is a big challenge and nanocomposites have been worldwide considered as promising materials.[1-15]

Nanocomposites can offer advantages when dealing with the following fuel cell key issues: optimization of the membrane-electrode-catalyst interface, preparation of membranes able to effectively operate above 100^{o}C and under external low humidification in fuel cells fed with hydrogen and preparation of membranes with low alcohol crossover.[36,37] Above 100^{o}C and under external low humidification most of the available membranes starts to dehydrate, requiring more complex operating conditions to compensate the consequent conductivity decrease. The motivations for operating at high temperatures are improved reaction kinetics, minimization of catalyst poisoning by CO, simplification of the heat and water

(humidification) management in the cell, improved gas transport and other issues associated with catalyst and design. In the present work, novel nanocomposite membranes were prepared with sulfonated polyoxadiazole and different amounts of sulfonated dense and mesoporous (MCM-41) silica particles aiming the application as high temperature polymer electrolyte fuel cells. Sulfonated polyoxadiazole was selected based on its excellent thermal and mechanical stability as well as high proton conductivity values with good perspectives of application at low humidity conditions.[11,38] Experiments were performed at 120°C and under 25% RH, which are the targets of the automotive industry.

2. Experimental Section

2.1. Materials. Dicarboxylic acid 4,4'-diphenylether, DPE (99%, Aldrich), Dimethyl sulfoxide, DMSO (>99%, Aldrich), hydrazine sulfate, HS (>99%, Aldrich), sodium hydroxide, NaOH (99%, Vetec), poly(phosphoric acid), PPA (115% H_3PO_4, Aldrich), phosphoric acid (85%, Aldrich). All chemicals were used as received.

2.2. Filler functionalization. Functionalized silicas and the mesoporous silica were synthesized and characterized as described elsewhere.[4,39] The dense sulfonated silica particles were prepared by functionalization of aerosil silica nanoparticles (7 nm, 380 g/m^2) in two steps. First, a bromophenyl group was introduced onto the silica surface by silanation reaction of bromophenyltrimethoxysilane at 60°C for 3 days, and then sulfonated aromatic bishydroxy compounds were grafted onto the silica surface by nucleophilic substitution reaction.[4] The mesoporous sulfonated silica particles (SO_3H-MCM-41) were functionalized using 3-mercaptopropyltrimethoxysilane at 0°C for 22h and with subsequent oxidation of the incorporated thiol groups to sulfonic acid groups using H_2O_2 at room temperature for 48h.[39]

2.3. Synthesis of sulfonated poly(diphenyether-1,3,4-oxadiazole). The synthesis condition has been selected considering previously reported synthesis method for sulfonated polyoxadiazoles with high molecular weight and high sulfonation level (S/C 0.103).[11,40,41] The

typical polymerization had the following steps: initially PPA was added to the flask and heated up to 100°C under dry argon atmosphere. Then, HS was added to the PPA and homogenized through stirring and heating of the reaction medium. After reaching the reaction temperature (160 °C), DPE was added to the flask. The molar dilution rate (PPA/HS) and the molar monomer rate (HS/DPE) were kept constant and equal to 10 and 1.2, respectively. After finishing the batch time of 5h, the reaction medium was poured into tepid water (containing 5% w/v of sodium hydroxide), for precipitation of the polymer. The pH of this precipitation bath was controlled by addition of additional amounts of 5 % (w/v) NaOH aqueous solutions. The final polymer yield was close to 100% regarding the limiting reactant DPE.

2.4. Membrane preparation. Homogeneous membranes were cast from solutions with a polymer concentration of 4 wt. % in DMSO. After casting, the DMSO was evaporated in a vacuum oven at 60°C for 24h. For further residual solvent removal, the membranes were immersed in water bath at 60°C for 48h and dried in a vacuum oven at 60°C for 24h. The final thickness of the membranes was about 50 μm. Nanocomposite membranes were prepared by adding 2.5-10 wt.% of functionalized filler (based on polymer content) into the 4 wt.% polymeric solution. The solution was stirred for 6h and cast on a glass plate at 60°C for solvent evaporation and dried following the same protocol described for the membranes prepared only with the polymer. The final thickness of the membranes was in the range 70 μm. The sulfonated membranes were converted into its acid form by immersing the cast membranes in 1.6M H_3PO_4 at room temperature for 24 h, followed by immersion in water for 2 x 24 h to ensure total leaching of residual phosphoric acid.

2.5. Membrane morphological investigation. The membrane morphology was observed by scanning electron microscopy (SEM) type LEO 1550VP. The samples were previously coated with gold in a sputtering device. Atomic force microscopy (AFM) of samples was done by using a Multi Mode Scanning Probe Microscope Model with a nanoscope IV

controller by Digital Instruments Inc. (Veeco Metrology Group). AFM observations were carried out in air at ambient conditions (25 °C) using tapping mode probes with constant amplitude. Micrographs in topographic and phase contrast modes were obtained.

2.6. Thermal and mechanical analysis. Thermogravimetric analysis (TGA) experiment was carried out in a Netzsch 209 TG, equipped with a TASC 414/3 thermal analysis controller. The film sample, under nitrogen atmosphere, was heated from 100 to 700°C at 10°C/min. Dynamic mechanical thermal analysis (DMTA) was used for determination of glass transition temperature (T_g), storage modulus (E'), loss modulus (E'') and loss tangent (Tan δ). DMTA was performed using a TA instrument RSA 2 with a film tension mode at a frequency of 1Hz and 0.1 N initial static force. The temperature was varied from 25 to 500 °C at a heating rate of 2°C/min and at a constant strain of 0.05%. Tensile testes were conducted on Zwick-Roell equipment according to the ASTM D882- 00 and operating at a cross-head speed of 5 mm min^{-1} at room temperature. The reported values correspond to an average of five specimens.

2.7. Conductivity of silica pellets. Ionic conductivity was measured in the frequency range 1-10^6 Hz with an oscillating voltage of 100 mV. The pellets of 8 mm in diameter and 0.5-1 mm in thickness were prepared by pressing the sulfonated silicas. The pellets were placed between two thin graphite slices and then put into a PTFE specimen holder where the pellet is clamped between two sintered metal electrodes. Measurements were performed with a flow cell purged with wet gas; the relative humidity was controlled by setting the temperature of a water reservoir heated at suitable temperature between 45 and 140°C.

2.8. Proton Conductivity of Membranes. Proton conductivity was measured by the AC impedance spectroscopy in the frequency range 10-10^6 Hz at signal amplitude ≤ 100 mV and obtained from the impedance modulus at zero phase shift (high frequency side) with 5 to 25% of relative humidity (RH). Measurements were performed with a flow cell purged with wet nitrogen; the relative humidity was controlled by bubbling nitrogen gas in water heated at a

suitable temperature between 49 and 81°C. The impedance measurements were carried out on stacks containing up to five membranes (cumulative thickness around 400 μm). The spectrometer used was a Zahner IM6 electrochemical workstation.

3. Results and Discussion

For the preparation of the nanocomposite polyoxadiazole membranes four different fillers were used, being three of them constituted of dense sulfonated silica particles and one of mesoporous sulfonated silica particles. The structures of the sulfonated silicas are depicted in Table 1. Because of the size (1-5 μm) of the SO_3H-MCM-41 particles, microcomposite polyoxadiazole membranes could be prepared only. An interesting aspect of the use of the SO_3H-MCM-41 particle is its nanoporous structure and the presence of functionalized groups within the porous, as characterized elsewhere.[39] The hexagonal structure of mesoporous Si-MCM-41 with a pore diameter d of 3 nm and lattice constant a_0 of 4.53 nm and is shown in Fig. 1 (a). A proposed attaching of the $SiO_2OHC_3H_6$-SO_3H group onto the pore wall of Si-MCM-41 is shown in Fig. 1 (b-c).

The dense sulfonated silica particles have been used as fillers in two different polymeric matrices, sulfonated polyetherketone[4] and fluorinated polyoxadiazole.[42] In all cases, enhanced proton conductivity values have been obtained when the sulfonated silica particles were added into the polymeric matrices. Based on the level of sulfonation of the groups incorporated onto the silica surface,[4] the silica-sulfone was expected to lead to better proton conductivity values. Contrary to expectations, the silica-telechelic led to a significant improvement in proton conductivity.[4] The higher enhancement was attributed to the basic nitrogen sites of the telechelic structure, which may favor additional points for proton jumps. In order to obtain a deeper insight into the influence of the ionic conductivity of the filler on the final conductivity of the composite membrane, in this manuscript the ionic conductivities of these sulfonated silica were characterized. Fig. 2 shows the ionic conductivities obtained for the pellets of

sulfonated silicas measured under different relative humidity conditions. Data for the SO_3H-MCM-41[39] filler are also included in Fig. 2 for comparison.

As expected, the conductivity of the fillers has a strong dependence on the level of hydration and temperature. The high conductivity values at RH=100% (up to 10^{-2} S cm^{-1}) sharply decrease upon dehydration (up to 10^{-5} S cm^{-1}). The higher conductivity obtained for the silica-fluorpropane in all conditions may be attributed to its acidity. The electronegative fluorine atoms probably have significant contribution to the formation of hydrogen bonds with water. The low proton conductivity values obtained for the SO_3H-MCM-41 at low relative humidities probably results from the non-uniform distribution of sulfonated ions in the pores (Fig.1.b),[43] which is very important under minimal hydration conditions. The mechanism of proton transport is a result of proton jumps between stationary donor and acceptor sites (Grotthus mechanism) and/or a result of the free mobility of H_3O^+ cations (vehicular mechanism), which are formed by coordination of protons to H_2O or acid molecules. Under minimal hydration conditions, the protons move from site to site with minor influence of diffusible H_2O molecules. Therefore, the distance between the hopping sites and the uniformity of these sites are very important. At temperatures above 120°C and 100% RH, all sulfonated silicas have similar conductivity values (ca. 10^{-2} S cm^{-1}), indicating the good water retention capacity of these fillers as well as their conductive nature.

The ionic conductivity data at 120 °C and under 5-25% RH of the composite membranes containing 5 wt.% of fillers are shown in Fig. 3. To analyse the effect of each filler without the influence of eventual residual phosphoric acid used for converting the sulfonated membrane into its acid form, the conductivity of the membranes in salt form was measured. All composite membranes had higher proton conductivity than the pristine polymer membrane in all range of relative humidity. The significant difference between conductivity data of composite membranes and the pristine polymer membrane at low relativity humidity (e.g. 15 RH%) is probably a consequence of the better water retention capacity of the

composite membranes conferred by the sulfonated silicas. Considering the error bar for the measurements, no significant difference among the fillers could be observed, except for the nanocomposite prepared with silica-telechelic. Similar to the systems based on sulfonated poly(ether ether ketone),[4] a significant enhancement on conductivity values was observed for the nanocomposite prepared with silica-telechelic. For instance, the ionic conductivity at 120°C and 15% RH for the membrane containing 5 wt.% silica-telechelic exceeds the value obtained for the pristine polymer membrane by one order of magnitude. Taking into account the lower conductivity values of this silica (Fig. 2) before the incorporation in the membrane, this result supports once more that the amphoteric character of the sulfonated telechelic attached to the surface of the silica containing both basic nitrogen sites as well as acid sulfonic acids favor additional points for proton jumps. The lower influence of conductivity on the relative humidity for the nanocomposite membrane prepared with silica-telechelic also reinforces the favored Grotthus mechanism by the telechelic structure.

All nanocomposite membranes prepared with sulfonated dense silica particles were transparent, indicating the absence of significant particles agglomerates. On the other hand, because of the large particle sizes of the sulfonated mesoporous silica particles, SO_3H-MCM-41, which are around 1-5 μm, turbid microcomposite membranes could be prepared only. The homogeneity of all composite membranes was confirmed by the SEM images. As shown in Fig. 4 (a-d), well homogeneous nanocomposite membranes without particle agglomerates were prepared with sulfonated dense silica particles. A homogeneous distribution of SO_3H-MCM-41 can also be observed even though the particles are quite large.

AFM observations were used to confirm that the sulfonated dense silica particles are homogeneously distributed. In the phase contrast mode, the effect of the topography is much smaller and the influence of other parameters like the difference in hardness of inorganic particle and organic polymer matrices can be clearly identified. In this case, the inorganic particles can be differentiated and assigned to the bright areas. The analysis of the AFM

images (Fig. 5) of the nanocomposite membranes containing sulfonated silicas confirms the particle nanosizes in the range 10-15 nm for the nanocomposite containing 5 wt.% silica-fluorpropane (a), 20-67 nm for the nanocomposite containing 5 wt.% silica-telechelic (b) and 20-75 nm for the nanocomposite containing 10 wt.% silica-telechelic (c), respectively. By increasing the filler concentration the occurrence of agglomerates increases.

The particle size has an effect on the mechanical properties of the composite membranes. Mechanical properties of the nanocomposite membranes prepared with dense sulfonated silicas were kept unchanged, while for the microcomposite membrane prepared with 5-10 wt.% SO_3H-MCM-41 the mechanical properties slightly decreased (Tables 1 and 2). The T_g values of the composite membranes slightly increased with addition of sulfonated silica, which might be caused by the hydrogen bonding between the sulfonic acid groups of the silica and the polyoxadiazole. Interaction between the sulfonated silicas and the polyoxadiazole results in constrained polymer chains in the vicinity of the inorganic particles. The depression in tan δ indicates the reduction of chain mobility during the glass transition,[7,44] where the relative peak height is proportional to the volume of the constrained chains. Fig. 6 clearly shows the reduction of the relative peak height of tan δ and the increase of the T_g values with increasing amount of sulfonated silicas. This result supports once more the very well dispersed silica particles within the polymeric matrix. On the other hand, for 10 wt.% SO_3H-MCM-41 aggregation of the large size particles leads to a decrease of mechanical properties as well as insignificant change in the T_g value (Table 2).

Thermal stability of composite membranes prepared with 2.5-10 wt.% of silica-telechelic and SO_3H-MCM-41 particles was analyzed by TGA. As shown in Fig. 7, the pristine polyoxadiazole membrane has two distinct regions of weight loss. The first occurs between 250 and 370°C with an approximate weight loss of 4% due to decomposition of sulfonic acid groups. The second region starting at 469°C is associated with the loss of volatiles caused by the degradation of the polyoxadiazole. These two weight loss temperatures slightly shifted

toward higher temperatures with addition up 5 wt.% loading of silica-telechelic, while for 10 wt.% loading of silica-telechelic they remained unchanged. The addition of 2.5 wt.% of SO_3H-MCM-41 did not alter the degradation pattern of the pristine polyoxadiazole membrane. On the other hand, with 5 and 10 wt.% loading of SO_3H-MCM-41 the first region of weight loss shifted toward lower temperature, probably because of the lower interaction between the sulfonic acid groups of the large mesoporous silica particles and of the polyoxadiazole chains. As the sulfonic acid groups are more located inside the pores,[43] lower interactions with the polymer amphoteric groups are expected. This would also explain the slightly poorer mechanical properties.

Because of the better results observed for the nanocomposite membrane containing silica-telechelic, these membranes were converted into acid form and their proton conductivity values were measured as shown in Fig. 8. In the acid form, proton conductivity value of the nanocomposite membrane containing 5 wt.% silica-telechelic is only slightly higher than the observed for the pristine polymer membrane as a result of the already very high proton conductivity of the polymer (10^{-2} S cm^{-1}), which exceeds by more than three orders of magnitude of the silica-telechelic (Fig. 2). No appreciable difference in proton conductivity values for the membrane containing 2.5-5 wt.% silica-telechelic was observed. Combined with the mechanical tests, this result indicates insignificant difference in the membrane properties for this loading range. On the other hand, for the membrane containing 10 wt.% silica-telechelic proton conductivity markedly increases. The proton conductivity was 34 mS cm^{-1}, much higher than 17-21 mS cm^{-1}, the value for the pristine polymer membrane. Based on this result, 10 wt.% of silica-telechelic is considered here the optimal loading for this system.

Conclusions

Particle size and functionality of sulfonated silica particles play an important role when they are used as fillers for the development of polymer electrolyte nanocomposite membrane for

fuel cells. Though high conductivity values are obtained for the sulfonated silica particles containing fluorine atoms, sulfonated silica particles containing both basic nitrogen sites as well as acid sulfonic acids lead to a significant improvement of nanocomposite polyoxadiazole conductivity when inserted into the polymeric matrix. All nanocomposite membranes prepared with sulfonated dense silica particles were transparent, indicating the absence of significant particles agglomerates. On the other hand, because of the particle sizes of the sulfonated mesoporous silica particles SO_3H-MCM-41 particles (1-5 μm), turbid microcomposite membranes could be prepared only. Mechanical properties of the nanocomposite membranes prepared with dense sulfonated silicas were kept unchanged, while for the microcomposite membrane prepared with 5-10 wt.% SO_3H-MCM-41 the mechanical properties slightly decreased. The T_g values of the composite membranes increased with addition of sulfonated silica, indicating interaction between the sulfonic acid groups of the silica and the polyoxadiazole. Constrained polymer chains in the vicinity of the inorganic particles were observed for both nanocomposite prepared with sulfonated silica particles and with mesaporous silica particles by the reduction of the relative peak height of tan δ. A proton conductivity of 0.034 S cm^{-1} at 120°C and 25% RH, which is around two-fold higher than the value of the pristine polymer membrane was obtained.

ACKNOWLEDGMENT. D. Gomes thanks the Helmholtz-Hochschul-Nachwuchsgruppe Projekt (VH-NG-323) for supporting this research. R. Marschall gratefully acknowledges a Georg-Christoph-Lichtenberg scholarship by the Ministry of Science and Culture of the German State of Lower Saxony, and financial support from the DFG (WA 1116/15, SPP 1181). The authors thank H. Böttcher for the dynamic mechanical thermal analyses and tensile tests, S. Nowak for the TGA measurements, K. Prause for the SEM images and S.

Bolmer for the AFM topographies. The cooperation was initiated in the frame of the CARISMA Coordination Action.

FIGURE CAPTIONS

Figure 1. Hexagonal structure of mesoporous Si-MCM-41 (a), schematic loading of SO_3H groups within the pores of the Si-MCM-41 (where the colors correspond to: blue carbon, yellow sulfur, red oxygen, white hydrogen) (b), proposed attaching of $SiO_2OHC_3H_6$-SO_3H groups onto the pore wall of Si-MCM-41 (c).

Figure 2. Dependence of ionic conductivity on the temperature for different fillers measured at relative humidity (RH) equal to 100 % (a), 50 % (b) and 0% (c).

Figure 3. Ionic conductivity of polyoxadiazole nanocomposite membranes as a function of relative humidity measured at 120°C.

Figure 4. SEM micrographs of the cross-section of the polyoxadiazole membrane (a) and of the polyoxadiazole nanocomposite membranes containing 5 wt.% silica-fluorpropane (b), 5 wt.% silica-telechelic (c), 10 wt.% silica-telechelic (d), 2.5 wt.% SO_3H-MCM-41 (e) and 5 wt.% SO_3H-MCM-41 (f).

Figure 5. AFM images of the polyoxadiazole nanocomposite membranes surfaces containing 5 wt.% silica-fluorpropane (a), 5 wt.% silica-telechelic (b) and 10 wt.% silica-telechelic (c). (Left) Tapping mode AFM topography. (Right) Phase mode AFM image of the same area.

Figure 6. Tan δ vs temperature as measured by DMTA at 1 Hz for the nanocomposites containing sulfonated silica (a) and sulfonated mesoporous silica (b).

Figure 7. TGA curve for the polyoxadiazole nanocomposite membranes containing silica-telechelic and SO_3H-MCM-41.

Figure 8. Proton conductivity of polyoxadiazole nanocomposite membranes as a function of silica-telechelic content measured at 120°C and 25 % RH.

TABLES

Table 1. Filler structures, T_g values and mechamical properties of polyoxadiazole nanocomposites containing 5 wt.% sulfonated silica

Table 2. T_g values and mechamical properties of polyoxadiazole nanocomposites containing different contents of sulfonated silica (silica-telechelic) and mesoporous silica (SO_3H-MCM-41).

REFERENCES

(1) Croce, F.; Appetecchi, G. B.; Persi, L.; Scrosati, B. *Nature* **1998**, *394*, 456 - 458.

(2) Kanamura, K.; Mitsui, T.; Munakata, H. *Chem. Mater.* **2005**, *17*, 4845-4851.

(3) Chen, Z.; Holmberg, B.; Li, W.; Wang, X.; Deng, W.; Munoz, R.; Yan, Y. *Chem. Mater.* **2006**, *18*, 5669-5675.

(4) Gomes, D.; Buder, I.; Nunes, S. P. *Journal of Polymer Science Part B: Polymer Physics* **2006**, *44*, 2278-2298.

(5) Gomes, D.; Nunes, S. P.; Peinemann, K. V.; Stepahn, K.; Abetz, V. *German patent* DE 10 2005 056 564 A1, 2007.

(6) Saxena, A.; Tripathi, B. P.; Shahi, V. K. *J. Phys. Chem. B.* **2007**, *111*, 12454-12461.

(7) Chuang, S.-W.; Hsu, S. L.-C.; Liu, Y.-H. *Journal of Membrane Science* **2007**, *305*, 353-363.

(8) Lee, C. H.; Min, K. A.; Park, H. B.; Hong, Y. T.; Jung, B. O.; Lee, Y. M. *Journal of Membrane Science* **2007**, *303*, 258-266.

(9) Su, Y.-H.; Liu, Y.-L.; Sun, Y.-M.; Lai, J.-Y.; Wang, D.-M.; Gao, Y.; Liu, B.; Guiver, M. D. *Journal of Membrane Science* **2007**, *296*, 21-28.

(10) Wilhelm, M.; Jeske, M.; Marschall, R.; Cavalcanti, W. L.; Tolle, P.; Kohler, C.; Koch, D.; Frauenheim, T.; Grathwohl, G.; Caro, J.; Wark, M. *Journal of Membrane Science* **2008**, *in Press*.

(11) Gomes, D.; Roeder, J.; Ponce, M. L.; Nunes, S. P. *Journal of Power Sources* **2008**, *175*, 49-59.

(12) Pereira, F.; Vallé, K.; Belleville, P.; Morin, A.; Lambert, S.; Sanchez, C. *Chem. Mater.* **2008**, *in press*.

(13) Rhee, C.H.; Kim, H.K.; Chang, H.; Lee, J.S. *Chem. Mater.* **2005**, *17*, 1691-1697.

(14) Karthikeyan, C. S.; Nunes, S. P.; Prado, L. A. S. A.; Ponce, M. L.; Silva, H.; Ruffmann, B.; Schulte, K. *Journal of Membrane Science* **2005**, *254*, 139-146.

(15) Yamada, M.; Li, D.; Honma, I.; Zhou, H. *J. Am. Chem. Soc.* **2005**, *127*, 13092-13093.

(16) Merkel, T. C.; Freeman, B. D.; Spontak, R. J.; Z. He, I. P.; Meakin, P.; Hill, A. J. *Science* **2002**, *296*, 519-522.

(17) Jeong, H.-K.; Krych, W.; amanan, H.; Nair, S.; Marand, E.; Tsapatsis, M. *Chem. Mater.* **2004**, *16*, 3838-3845.

(18) Mahajan, R.; Koros, W. J. *Ind. Eng. Chem. Res.* **2000**, *39*, 2692-2696.

(19) Fritsch D.; Peinemann K.V.; de F. Gomes D.; *German Patent* DE102005017195 B4 2006.

(20) Gomes, D.; Nunes, S. P.; Peinemann, K.-V. *Journal of Membrane Science* **2005**, *246*, 13-25.

(21) Dzenis, Y. *Science* **2008**, *319*, 419-420.

(22) Balazs, A. C.; Emrick, T.; Russell, T. P. *Science* **2006**, *314*, 1107 - 1110.

(23) Qin, Y.; Wang, X.; Wang, Z. L. *Nature* **2008**, *451*, 809-813.

(24) Wang, Y.; Herron, N. *Science* **1996**, *273*, 632 – 634

(25) Ho, P. K. H.; Thomas, D. S.; Friend, R. H.; Tessler, N. *Science* **1999**, *285*, 233 - 236.

(26) Ji, X.; Hampsey, J. E.; Hu, Q.; He, J.; Yang, Z.; Lu, Y. *Chem. Mater.* **2003**, *15*, 3656 - 3662.

(27) Bragança, F. d. C.; Valadares, L. F.; Leite, C. A. d. P.; Galembeck, F. *Chem. Mater.* **2007**, *19*, 3334-3342.

(28) Uhl, F. M.; Davuluri, S. P.; Wong, S.-C.; Webster, D. C. *Chem. Mater.* **2004**, *16*, 1135-1142.

(29) Ciprari, D.; Jacob, K.; Tannenbaum, R. *Macromolecules* **2006**, *39*, 6565 -6573.

(30) Zhu, J.; Morgan, A. B.; Lamelas, F. J.; Wilkie, C. A. *Chem. Mater.* **2001**, *13*, 3774-3780.

(31) Yang H H. *Aromatic High-Strength Fibers*. John Wiley&Sons: New York, 1989.

(32) Cassidy, P. E., *Thermally Stable Polymers: Synthesis and Properties*. Marcel Dekker Inc.: New York, 1980.

(33) Nanjan, M. J., *Encyclopedia of Polymer Sci. and Engineering*. John Wiley&Sons: New york, 1987; Vol. 12.

(34) Helmholtz Association's Annual Report 2007, *Jack of all trades from the polymer lab*, Bonn, 2007; 47-48.

(35) Gomes D.; Abetz V.; Kannan B.; Dietzel W; *German patent application* 10 2007 007 879.1.

(36) Alberti, G.; Casciola, M. *Annu. Rev. Mater. Res.* **2003**, *33*, 129-154.

(37) Li, Q.; He, R.; Jensen, J. O.; Bjerrum, N. J. *Chem. Mater.* **2003**, *15*, 4896-4915.

(38) Gomes, D.; Roeder, J.; Ponce, M. L.; Nunes, S. P. *Journal of Membrane Science* **2007**, *295*, 121-129.

(39) Marschall, R.; Bannat, I.; Caro, J.; Wark, M. *Microporous and Mesoporous Materials* **2007**, *99*, 190-196.

(40) Gomes, D.; Borges, C. P.; Pinto, J. C. *Polymer* **2001**, *42*, 851-865.

(41) Gomes, D.; Borges, C.; Pinto, J. C. *Polymer* **2004**, *45*, 4997-5004.

(42) Gomes, D.; Nunes, S. P. *Journal of Membrane Science* **2008**, *in press*.

(43) Marschall, R.; Rathouský, J. í.; Wark, M. *Chem. Mater.* **2007**, *19*, 6401-6407.

(44) Rao, Y.; Pochan, J. M. *Macromolecules* **2007**, *40*, 290-296.

(Table 1)

Polymer Sample + 5 wt.% sulfonated silica 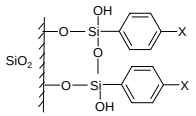	S/C [a]	Young's modulus (GPa)	Tensile strength (MPa)	Elongation (%)	T_g (°C) [b] E''	T_g (°C) [b] Tan δ
-	0.103	3.07 ± 0.30	145 ± 12.1	49.5 ± 16.8	416	430
Silica-sulfone X= 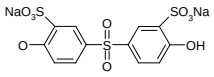	0.120	3.04 ± 0.12	148 ± 15.0	63.0 ± 10.8	425	445
Silica-fluorpropane X = 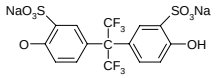	0.106	3.17 ± 0.19	144 ± 15.5	53.4 ± 17.3	430	445
Silica-telechelic X= 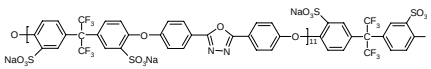	0.104	3.10 ± 0.03	118 ± 16.7	33.6 ± 11.9	425	445

[a] determined by elemental analysis, [b] Glass Transition temperature measured by DMTA.

(Table 2)

Polymer Sample + filler	T_g (°C) [a]		T_{d10} (°C) [b]	Residue (%) [c]	Young's modulus (GPa)	Tensile strength (MPa)	Elongation (%)	Storage modulus (GPa)	
	E''	Tan δ						at 100 °C	at 300 °C
-	416	430	469	54	3.07 ± 0.30	145 ± 12.1	49.5 ± 16.8	4.69 ± 0.01	3.11 ± 0.04
Silica-telechelic									
2.5 wt. %	425	445	474	55	3.27 ± 0.38	141 ± 18.9	42.4 ± 10.2	3.99 ± 0.47	2.83 ± 0.10
5 wt. %	425	445	474	54	3.10 ± 0.03	118 ± 16.7	33.6 ± 11.9	4.48 ± 0.32	2.88 ± 0.16
10 wt. %	435	450	462	53	3.12 ± 0.12	124 ± 10.1	49.0 ± 13.2	4.58 ± 0.55	2.84 ± 0.27
SO_3H-MCM-41									
2.5 wt.%	430	450	472	53	3.06 ± 0.28	126 ± 14.3	50.6 ± 15.9	3.95 ± 0.03	2.98 ± 0.05
5 wt.%	435	450	467	54	2.91 ± 0.12	109 ± 6.78	37.1 ± 9.5	4.68 ± 0.10	3.20 ± 0.08
10 wt. %	420	440	429	53	-	-	-	3.43 ± 0.02	2.93 ± 0.02

[a] Glass Transition temperature measured by DMTA, [b] 10 % weight loss temperature measured by TGA, [c] Residue weight at 700 °C in N_2.

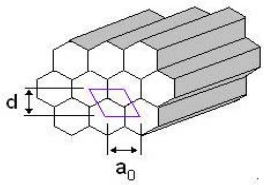

(a)

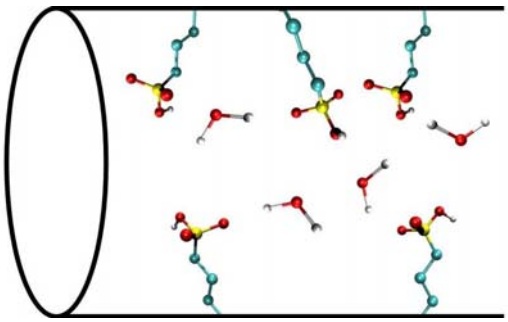

(b)

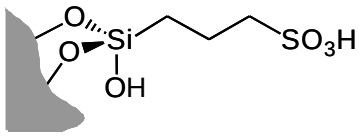

(c)

Figure 1

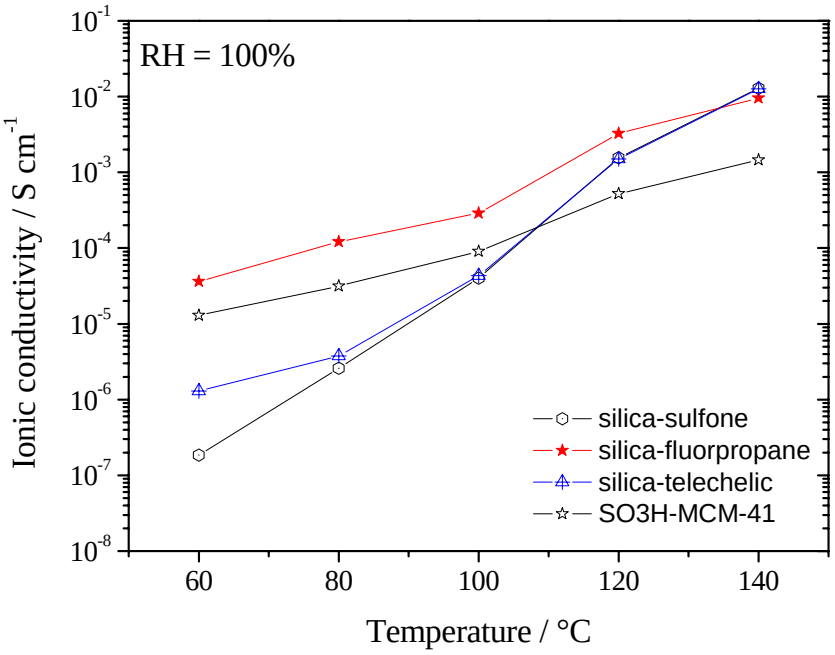
RH = 100%
Ionic conductivity / S cm-1
Temperature / °C
silica-sulfone
silica-fluorpropane
silica-telechelic
SO3H-MCM-41

(a)

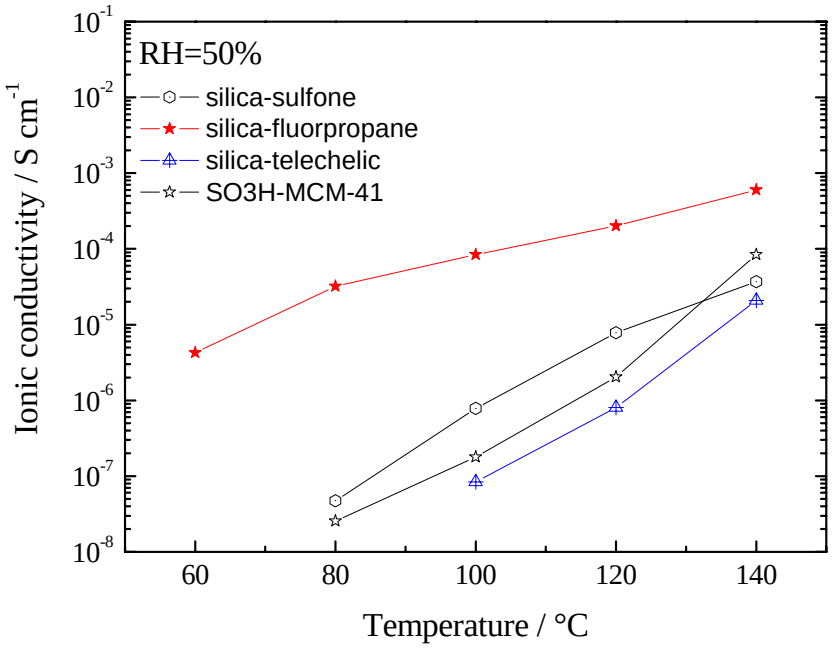
RH=50%
Ionic conductivity / S cm-1
Temperature / °C
silica-sulfone
silica-fluorpropane
silica-telechelic
SO3H-MCM-41

(b)

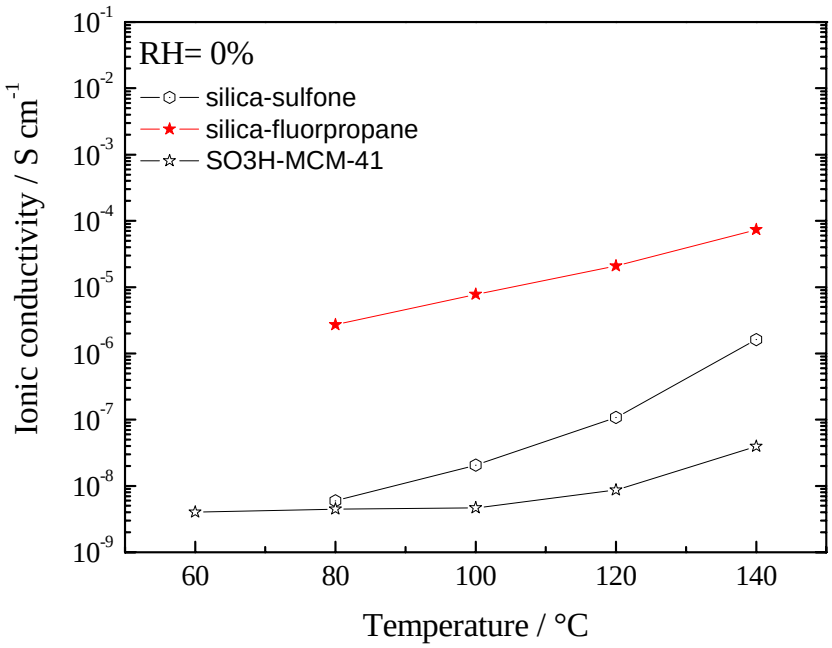
RH= 0%
silica-sulfone
silica-fluorpropane
SO3H-MCM-41
Ionic conductivity / S cm-1
Temperature / °C
10-1
10-2
10-3
10-4
10-5
10-6
10-7
10-8
10-9
60
80
100
120
140

(c)

(Figure 2)

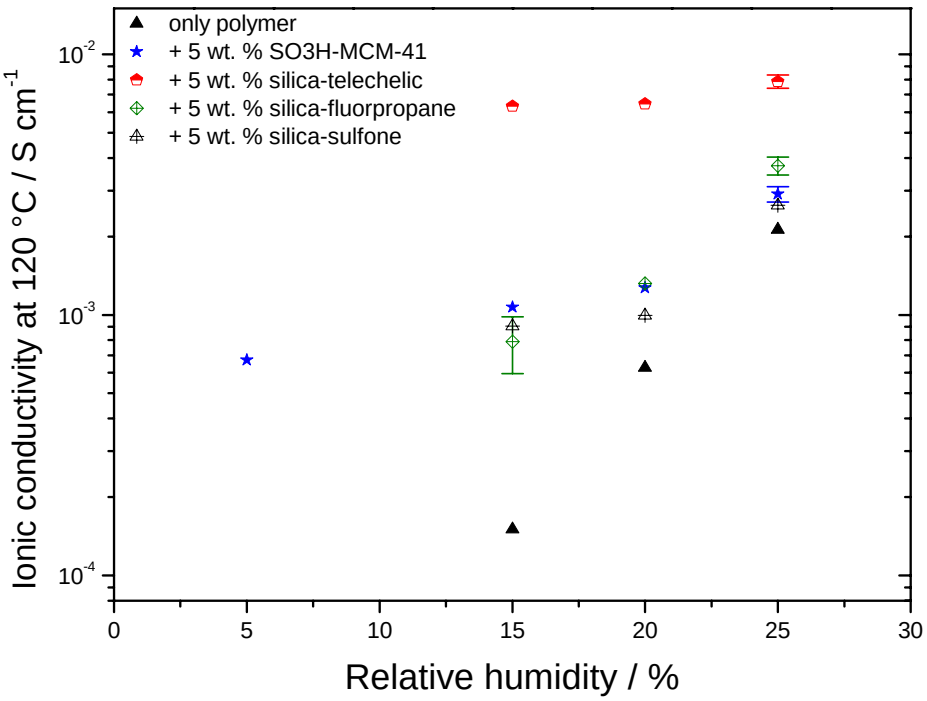
only polymer
+ 5 wt. % SO3H-MCM-41
+ 5 wt. % silica-telechelic
+ 5 wt. % silica-fluorpropane
+ 5 wt. % silica-sulfone
Ionic conductivity at 120 °C / S cm-1
10-2
10-3
10-4
0
5
10
15
20
25
30
Relative humidity / %

(Figure 3)

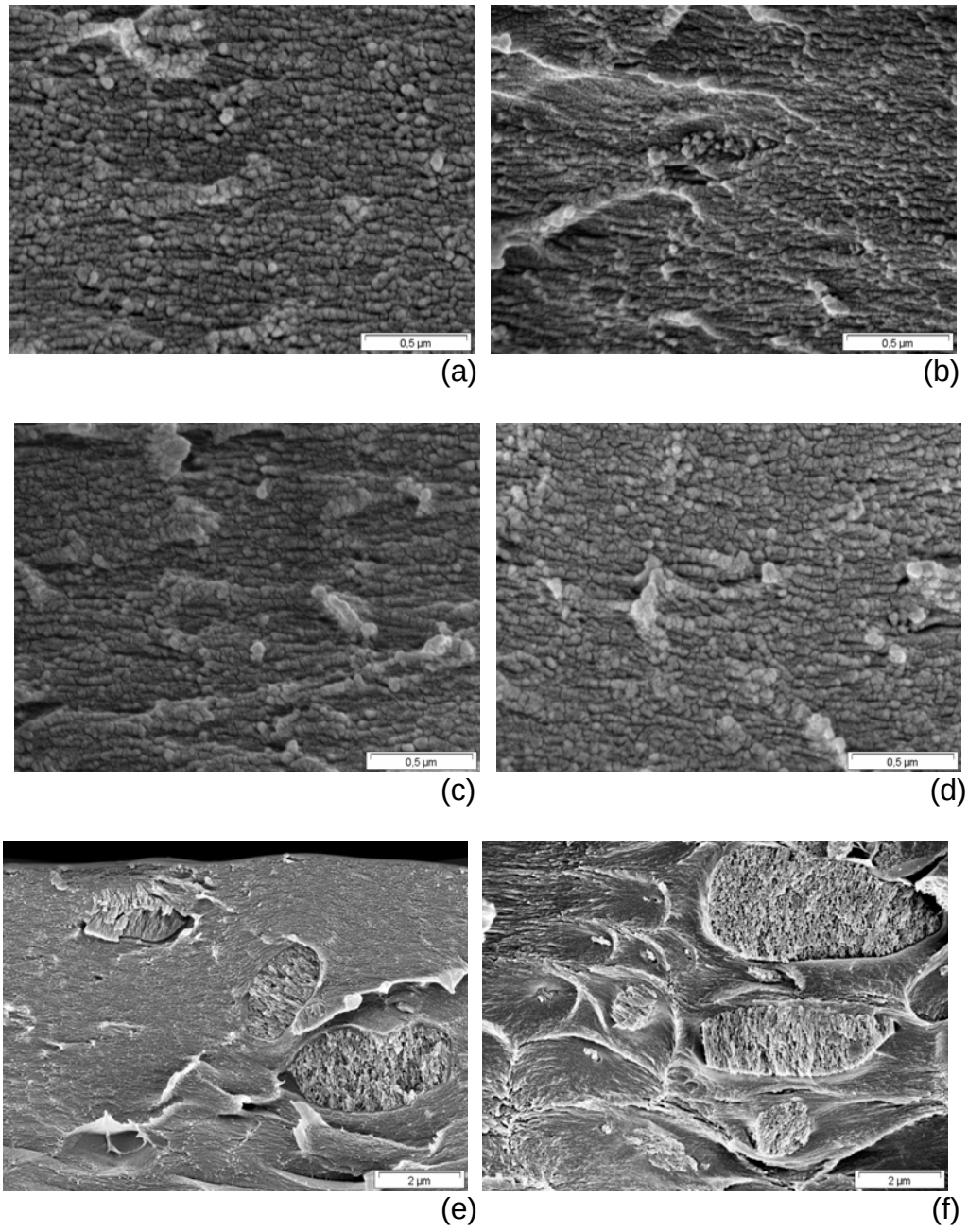

(Figure 4)

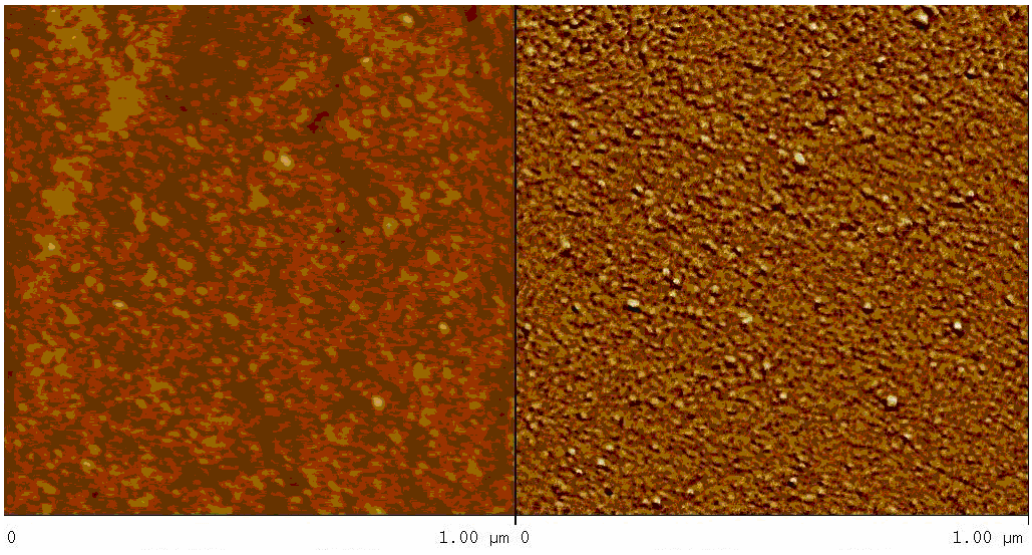

(a)

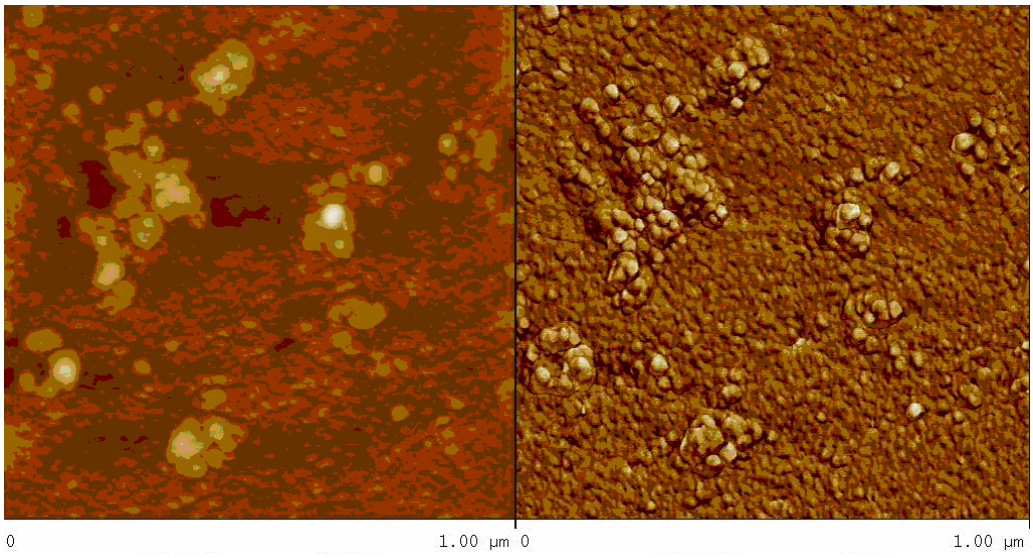

(b)

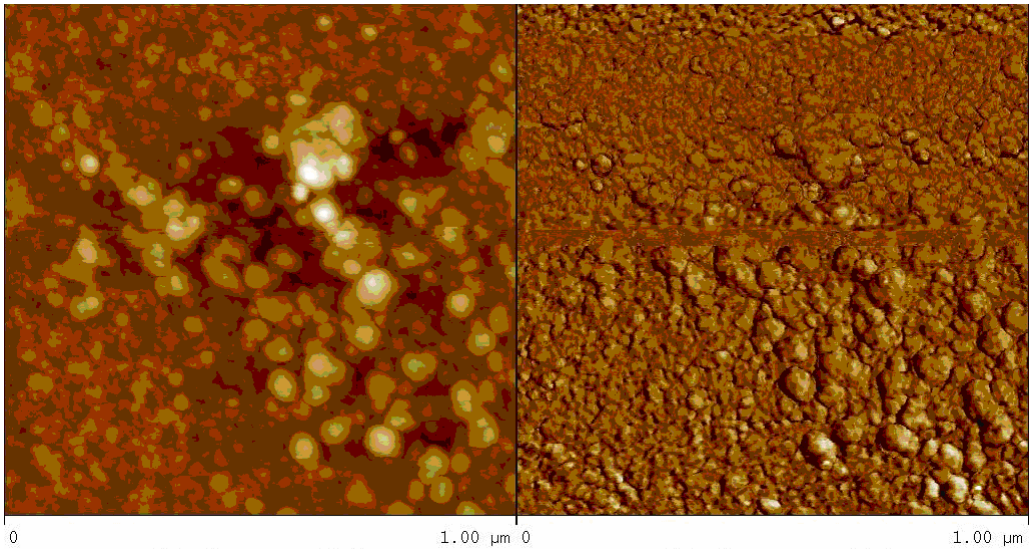

(c)

(Figure 5)

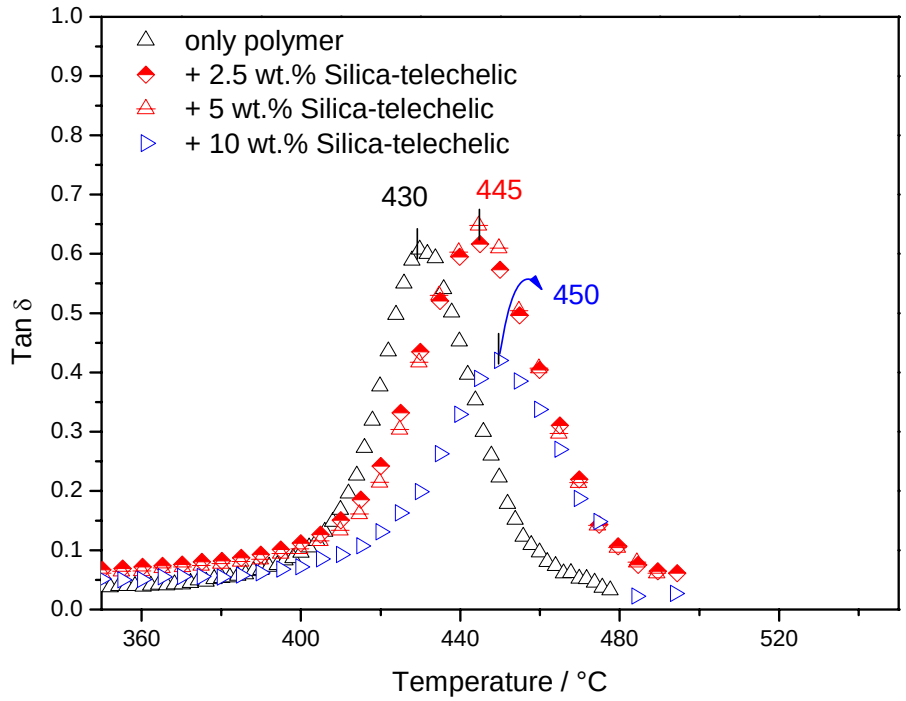
only polymer
+ 2.5 wt.% Silica-telechelic
+ 5 wt.% Silica-telechelic
+ 10 wt.% Silica-telechelic
430
445
450
Tan δ
Temperature / °C
1.0
0.9
0.8
0.7
0.6
0.5
0.4
0.3
0.2
0.1
0.0
360
400
440
480
520

(a)

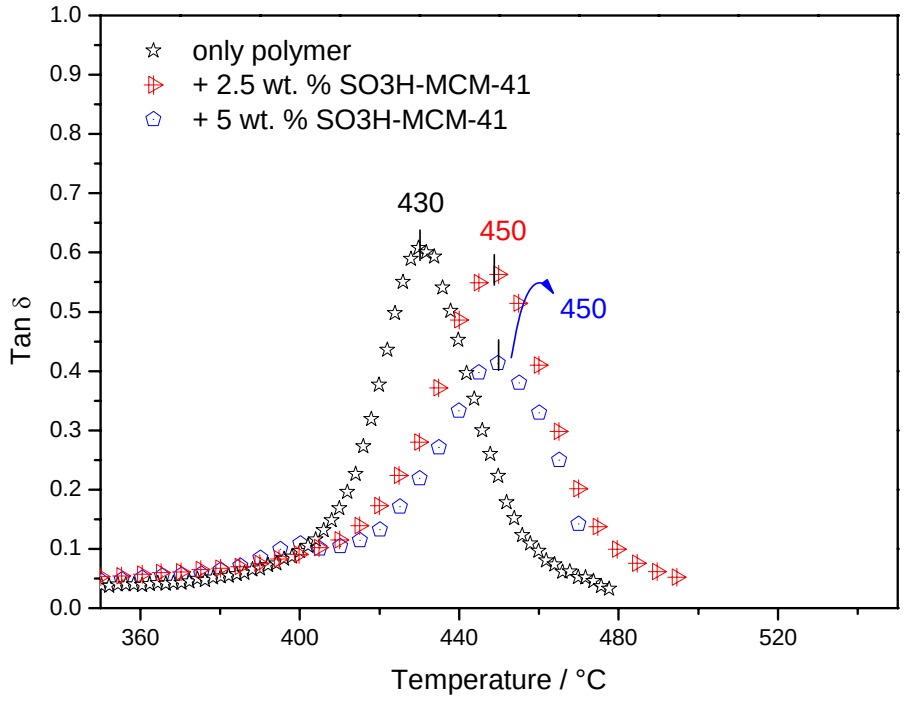
only polymer
+ 2.5 wt. % SO3H-MCM-41
+ 5 wt. % SO3H-MCM-41
430
450
450
Tan δ
Temperature / °C
1.0
0.9
0.8
0.7
0.6
0.5
0.4
0.3
0.2
0.1
0.0
360
400
440
480
520

(b)

(Figure 6)

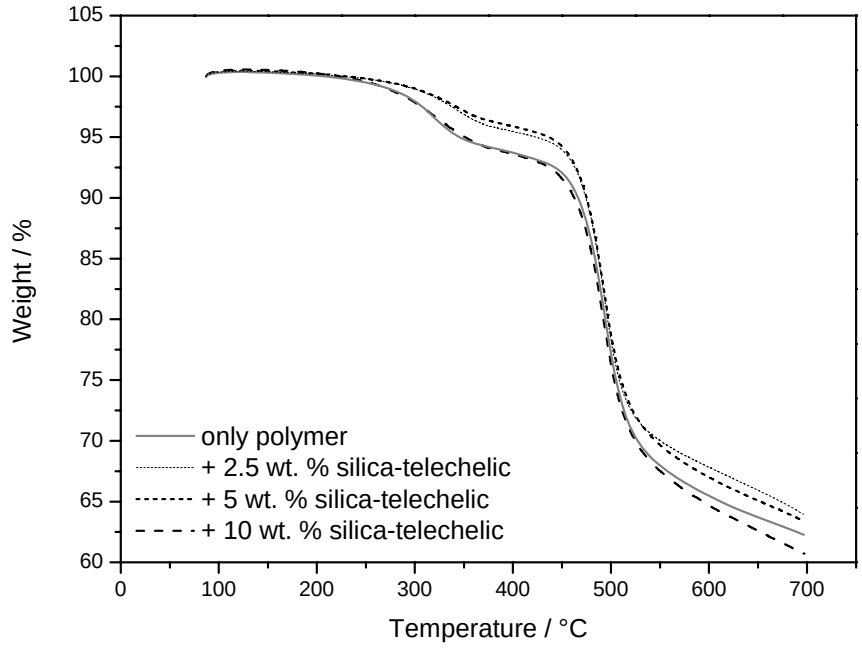
Weight / %
Temperature / °C
only polymer
+ 2.5 wt. % silica-telechelic
+ 5 wt. % silica-telechelic
+ 10 wt. % silica-telechelic

(a)

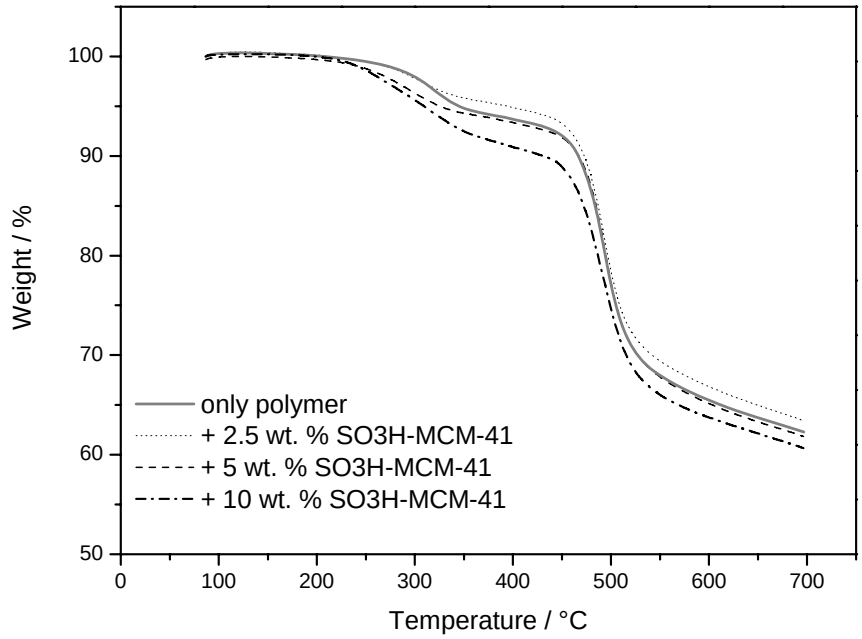
Weight / %
Temperature / °C
only polymer
+ 2.5 wt. % SO3H-MCM-41
+ 5 wt. % SO3H-MCM-41
+ 10 wt. % SO3H-MCM-41

(b)

(Figure 7)

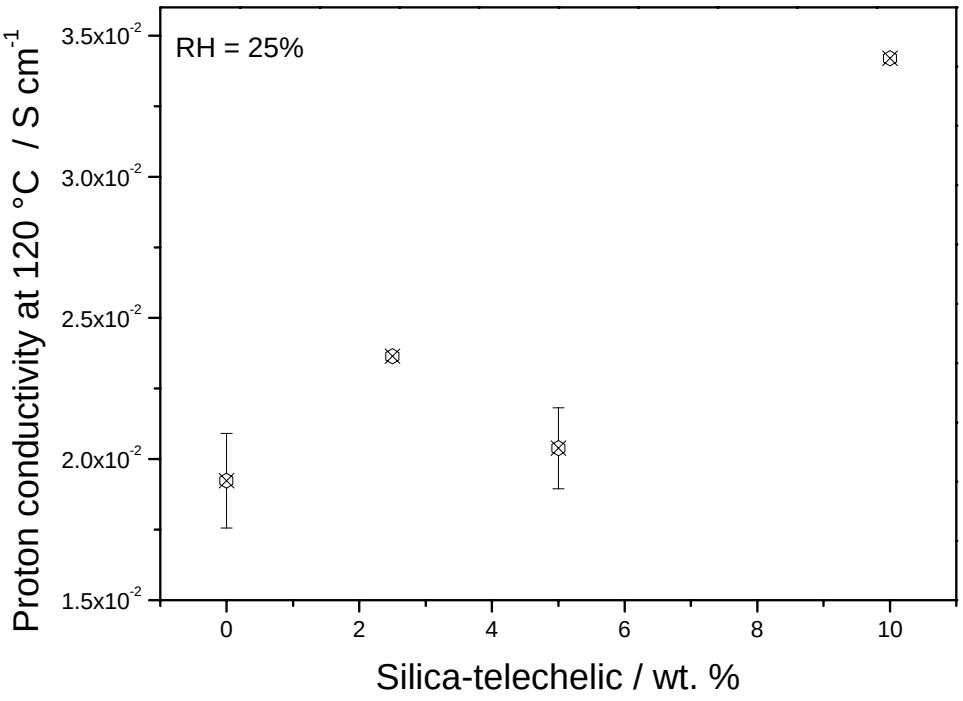
RH = 25%
Proton conductivity at 120 °C / S cm-1
3.5x10-2
3.0x10-2
2.5x10-2
2.0x10-2
1.5x10-2
0
2
4
6
8
10
Silica-telechelic / wt. %

(Figure 8)